Journal of the European Ceramic Society 19 (1999) 553–560

PII: S0955-2219(98)00249-0
0955-2219/99/$—see front matter

Characteristics of Ca-α-sialon—Phase Formation, Microstructure and Mechanical Properties

P. L. Wang,* C. Zhang, W. Y. Sun and D. S. Yan

The State Key Lab of High Performance Ceramics and Superfine Microstructure, Shanghai Institute of Ceramics, Chinese Academy of Sciences, 200050 Shanghai, China

(Received 2 June 1998; revised version received 19 September 1998; accepted 30 September 1998)

Abstract

Ca-α-Sialon ($Ca_xSi_{12-(m+n)}Al_{m+n}O_nN_{16-n}$) ceramics with extensive compositions on the line of Si_3N_4–CaO:3AlN (where $m=2n$) ranged from $x=0{\cdot}3$ up to $x=2{\cdot}0$ were fabricated by hot-pressing. An exploration for Ca-α-Sialon involving reaction sequences, phase compositions, cell dimensions, microstructure and mechanical properties was carried out in the present work. © *1999 Elsevier Science Limited. All rights reserved*

Keywords: sialon, microstructure-final, mechanical properties, hot pressing, transformation.

1 Introduction

α-Sialon (abbreviated as α′), iso-structure with α-Si_3N_4, contains two large isolated interstices where some large metal ions can be accommodated.[1] The general formula of α-Sialon is represented as $M_xSi_{12-(m+n)}Al_{m+n}O_nN_{16-n}$ with $x \leq 2$ and the elements M which have been reported to form α are Li, Ca, Mg, Y and most of the lanthanide elements. In comparison with β-Sialon (β′, $Si_{6-z}Al_zO_zN_{8-z}$), α' possesses high hardness because its structure consists of longer stacking sequence of ABCD and β′ has a stacking sequence of AB.[2] But more important, α′ provides the possibility to produce liquid-free (at least liquid-less) ceramics because the most of sintering additives, such as Y_2O_3 (Ln_2O_3), CaO and MgO can be adopted by α-Si_3N_4 structure, thus reducing the liquid phase remaining at the grain boundary. Therefore, α ceramics attracts researchers more attentions. In the last decades, the work on α′ ceramics has mainly focused on Y- and Ln-α-Sialon.[3,4] In these systems excellent mechanical properties — high hardness and reasonably high flexure strength have been achieved in α′-β′ multi-phase ceramics. However, in recent years, the Ln-α especially using those light rare earth elements (Nd and Sm) as modifier cations has been found to be unstable. During heat treatment in the temperature range of 1300–1500°C, the α′ formed during sintering would transform into β′.[5–7] This problem puzzles research scientists because this characteristic of α′ restricts its application at high temperatures. Therefore, the mechanism of α′→β′ phase transformation (or called decomposition of α′) has been widely studied. It seems there exist several effects to promote phase transformation and a lot of uncertainty still remains. In order to avoid this problem, Ca-α′ is a good candidate. In comparison with other α′, Ca-α′ can accommodate the largest concentration of the modifier cation ($x_{max}=1{\cdot}4$ for Ca-α′ and 0·6 to 1·0 for Ln from Nd to Yb).[3,8] The larger solubility of Ca^{2+} in the α′ structure has the benefit of making clean grain boundaries because the Ca^{2+} in the liquid phase can be mostly exhausted. From the economic point of view, the advantage of Ca-α′ is also obvious. The low quality of Si_3N_4 powder with CaO as impurity can be used and the chemical agent of CaO is much cheaper than Ln_2O_3. However, the study on Ca-α-sialon is relatively scarce. Based on the reason mentioned above, it is required to explore this potential Ca-α-sialon ceramics. The present work was carried out as an exploration for Ca-α-sialon involving reaction sequences, phase compositions, cell dimensions, microstructures and mechanical properties.

2 Experimental

The nominal compositions located on the join line Si_3N_4–CaO:3AlN (with a special formula of $Ca_xSi_{12-x}Al_{3x}O_xN_{16-x}$, i.e. $x=m/2=n$) with $x=$ 0·3 to 2·0 were explored in the present work. The x

*To whom correspondence should be addressed

values were selected to be 0·3, 0·6, 1·0, 1·2, 1·4, 1·6, 1·8 and 2 (named as C30, C60...C200). The starting powders used were Si_3N_4 (UBE-10, Japan, 2 wt%O), AlN (1·3 wt%O) and $CaCO_3$ (99·0%). The mixtures were milled for 1·5 h in an agate mortar under absolute alcohol. Powders were dried and then hot-pressed (20 MPa) at 1700–1750°C for 1 h in a graphite-resistant furnace under a flowing nitrogen of 1 atmosphere. Before reaching the holding temperature, the powder mixture was firstly kept at 1150°C for 0·5 h to complete the decomposition of $CaCO_3$. For the studies on reaction sequences, the composition with x value of 1 and the temperature range 1500–1750°C were selected. The holding time at the temperatures selected was 1 h. The bulk densities of the samples were measured by the Archimedes principle. Phase assemblages were characterized by X-ray diffraction using a Guinier-Hägg camera with Cu $K_{\alpha 1}$ radiation and Si as an internal standard. The measurement of X-ray film and refinement of lattice parameters were completed by a computer-linked line scanner (LS-18) system[9] and SCANPI, PIRUM[10] programs. The semi-quantitative estimation of the crystalline phases of samples was based on the calibration curves obtained from appropriate powder mixtures of every two phases. An X-ray diffractometer was also used for identifying the preferred orientation of α' grains in the hot-pressed samples. The Ca content in the α' grains was determined from element analysis using a SEM (KYKY 2000, China). The microstructure observation was performed under a JEM 200CX ATEM and JEM 2010CX HREM transmission electron microscope. Both SEM and TEM are equipped with energy dispersive spectrometer (Oxford/LINK ISIS 3·00). Hardness and indentation fracture toughness were measured by using a Vickers diamond indenter under a load of 100 N.

3 Results and Discussion

3.1 Formation of Ca-α-sialon and densification

Figure 1 shows the formation of Ca-α-sialon ($x=1$). For this particular composition, the formation of α' is nearly completed at 1600°C. Below this temperature (i.e. at 1500°C), unreacted α-Si_3N_4 and AlN still remain and an intermediate product, gehlenite ($2CaO{\cdot}Al_2O_3{\cdot}SiO_2$), occurs. With temperature increasing, α-Si_3N_4, AlN and gehlenite disappear and small amount of 21 R occurs. The presence of intermediate phase, gehlenite, is in agreement with the references.[11,12] The bulk densities and the phase assemblages of the compositions with x value from 0·3 to 2·0 (C30...200) are summarized in Table 1. As indicated, the density of samples increases with increasing the sintering temperature, but the increment diminishes with increasing x value of the compositions. The compositions with x value higher than 1 can be fully densified at 1700°C. However, at that temperature the compositions with low x value still contain unreacted α-Si_3N_4. The densification of Si_3N_4-based ceramics mainly depends on the liquid phase produced by the surface SiO_2 on Si_3N_4 powder and the oxide additives. The α' formation is also through dissolve and precipitation which in turn requires a certain amount of liquid phase. With increasing x value i.e. more CaO added, the composition is towards the liquid-rich side. Therefore, with the increasing of x value, the compositions becomes more easy to be densified. With the compositions shifting towards the terminal point CaO:3AlN (i.e. high x value), β' diminishes and AlN-polytypoids (or AlN) appear and gradually increase. This variation in phase compositions is in agreement with our previous work on the phase diagram of the Si_3N_4–CaO–AlN system.[8] The composition with $x=0{\cdot}3$ is located at the lowest limit of the α' solubility region below which there is a two phases region — α'-β' (or β-Si_3N_4). Therefore, the appearance of β' in the sintered composition ($x=0{\cdot}3$) is expected because some of the CaO is exhausted by the formation of the liquid phase and the actual quantity of Ca^{2+} entering into α' is less than 0·3. The top limit of Ca-α-sialon on the line Si_3N_4–CaO:3AlN is at $x=1{\cdot}4$, beyond which there is a multi-phase region—α-sialon, liquid and AlN-polytypoids or AlN. Recently, Hewett *et al.*[13] figured out the phase diagram of the Ca-α-sialon plane, i.e. the Si_3N_4–4/3(AlN:Al_2O_3)–1/2(Ca_3N_2):3AlN system (Fig. 2). As indicated in Fig. 2, on the right side of the α' region, there exist many very narrow compatibility triangles, each of which contains three phases—α', one type of AlN-polytypoids (15 R, 12 H, 21 R...) or AlN and liquid phase. When oxygen content in α' compositions

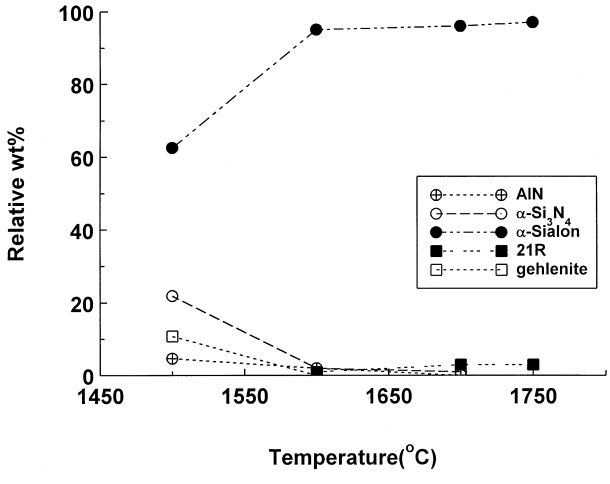

Fig. 1. Reaction sequences of Ca-α-sialon ($x=1{\cdot}0$).

Table 1. Density and phase present of Ca-α′ samples hot-pressed

Sample no.	*Density (g/cm³)*		*Phase present*[b]	
	1700°C/1 h	*1750°C/1 h*	*1700°C/1 h*[a]	*1750°C/1 h*
C30	2·86	3·02	α′ s; α w; β′ vw	α′ s; β′ mw; α vw
C60	3·07	3·17	α′ s; α w	α′ s; α tr.
C100	3·19	3·21	α′ s; 21 R vw	α′ s; 21 R vw
C140	3·21	3·21	α′ s; 21 R w	α′ s; 21 R mw
C160	—**	—	—	α′ s; 21 R mw
C180	—	—	—	α′ s; AlN m; 21 R w
C200	—	—	α′ s; AlN ms; 21 R w	—

[a]Taken from X-ray diffractometer.
[b]S = Strong.
M = Medium.
W = Weak.
**Not measured.

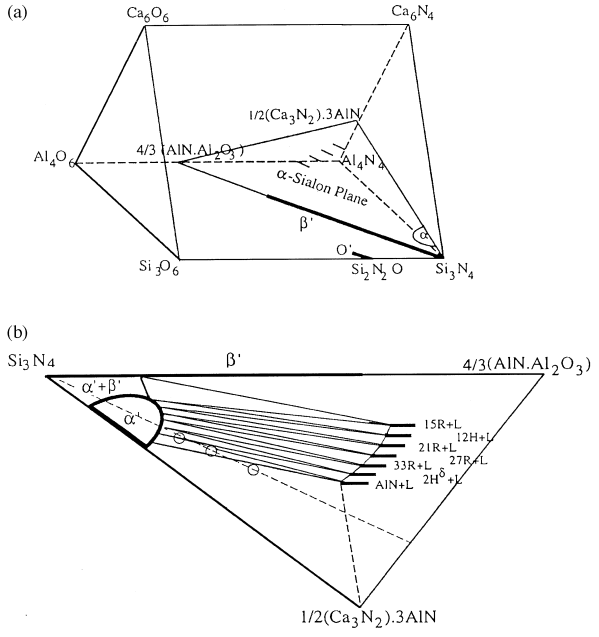

Fig. 2. (a) Representation of α-sialon plane in the Ca–Si–Al–O–N system and (b) phase relationships in Ca-α-sialon plane (the dash line crossing the α′ region represents the join line of Si_3N_4–CaO:3AlN and the dots on the line have no relationships with the present work).[13]

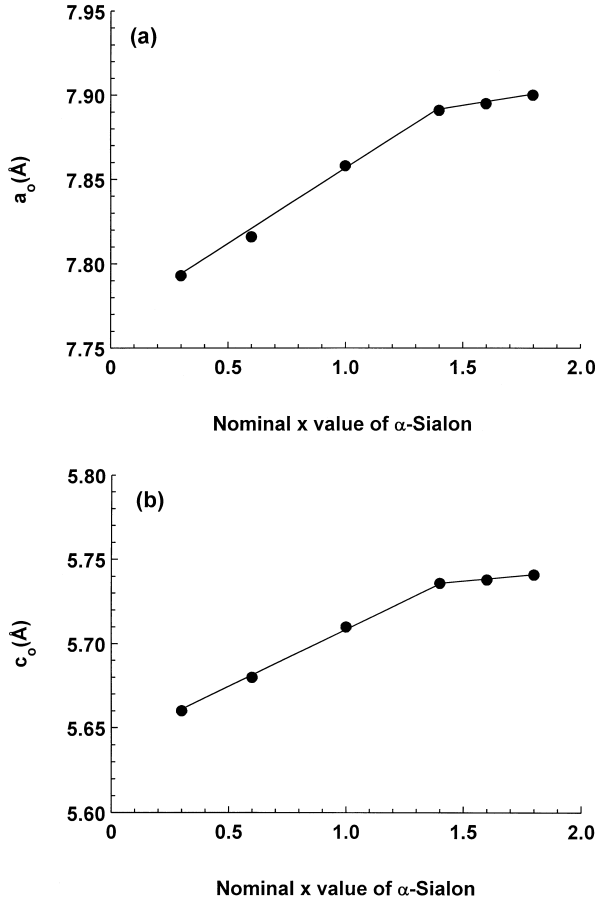

Fig. 3. Cell dimensions versus nominal α-sialon compositions: (a) *a* axis; (b) *c* axis.

decreases, the AlN-polytypoid, which is compatible with α′, is also towards oxygen-less. The oxygen content in AlN-polytypoids decreases in sequence of 15 R ($SiAl_4O_2N_4$), 12 H ($SiAl_5O_2N_5$), 21 R ($SiAl_6O_2N_6$)... until AlN. Actually, the compositions made by Si_3N_4, CaO and AlN as starting materials cannot be exactly located on the Si_3N_4–CaO:3AlN line, because the oxygen existing on the surface of the Si_3N_4 (2 wt%O) and AlN (1·3 wt%O) powder cannot be compensated without using Ca_3N_2 as starting material. The actual compositions slightly shift towards oxygen-rich and this composition line crosses the compatibility triangles involving 21 R, 27 R, and AlN. Based on this phase diagram, the appearance of 21 R and AlN in sequence in the samples with the compositions beyond the top boundary of the α′ can be understood.

3.2 Cell dimensions of Ca-α-sialon

The cell dimensions of α′ hot pressed at 1700 and 1750°C were determined and are listed in Table 2. Obviously, for the same composition of Ca-α-sialon, no difference in cell dimensions between 1700 and 1750°C was observed. It has been known that the liquid phase exhausts Ca^{+2} and makes the actual Ca^{+2} content in the α′ lower than the nominal

Table 2. Lattice parameters of Ca-α' with nominal and determined x value by EDX

X value		*Hot-pressed at 1700°C*			*Hot-pressed at 1750°C*		
Nom.[c]	*EDX*[b]	*a(Å)*	*c(Å)*	*V(Å³)*	*a(Å)*	*c(Å)*	*V(Å³)*
0·3	—[a]	7·7932(6)	5·6652(8)	297·97	7·7910(8)	5·6609(10)	297·58
0·6	0·4	7·8163(7)	5·6796(9)	300·50	7·8185(13)	5·6752(8)	300·44
1·0	0·7	7·8584(7)	5·7098(7)	305·37	7·8532(7)	5·7185(6)	305·42
1·2	0·76	7·8633(5)	5·7201(6)	306·30	—	—	—
1·4	0·9	7·8914(5)	5·7356(6)	309·32	7·8886(6)	5·7345(6)	309·05
1·6	—	7·8945(6)	5·7373(9)	309·68	—	—	—
1·8	—	7·8995(6)	5·7409(6)	310·25	—	—	—
2·0	—	7·9142(3)	5·7465(4)	311·70	—	—	—

[a]Not measured.
[b]Obtained from the specimens hot-pressed at 1700°C
[c]Nominal x value.

compositions. In order to know how much the Ca^{+2} content enters α' structure, the present work determined the Ca^{+2} content in α' grains by EDAX. As indicated in Table 2, the actual content of Ca^{+2} in α' grains is less than the nominal one. In the composition range of $x = 0{\cdot}3$–$1{\cdot}4$, the actual Ca^{+2} level in α' is around 70% of the added amount, i.e. with 30% of Ca^{+2} remaining in the glassy phase. The cell dimensions of α' versus the nominal x value indicate that with the increasing x value, the increment of cell dimensions becomes sluggish (see Fig. 3). There exists a critical point at around $x = 1{\cdot}4$ which changes the slopes of the lines. When the x value exceeds 1·4, more Ca^{+2} remains in the glassy phase of the sample. By using the determined x values instead of the nominal x values as variation, both the a_o and c_o values can keep within the straight lines, as shown in Fig. 4. Based on the established lines, the cell dimensions of $a_o = 7{\cdot}9142$ Å, $c_o = 5{\cdot}7465$ Å observed in composition C200 corresponds to an actual x value of around 1·0. That means only 50% of Ca^{+2} entering into α' structure for that composition. The expansion of cell dimensions in α' is mainly caused by the substitution of Si-N by Al-N and the variations with m and n were firstly reported by Hampshire *et al.*[1] as following:

$$\Delta a_o(\text{Å}) = 0{\cdot}045\, m + 0{\cdot}009\, n \qquad (1)$$

$$\Delta c_o(\text{Å}) = 0{\cdot}04\, m + 0{\cdot}008\, n \qquad (2)$$

In these early equations, the cell dimensions have no relationships with the modifier cation. Actually, the expansion of α' structure does have relevance with the species of the cation and recently the revisions for Y-,[14] Ln-[15] and Ca-α-sialons[11] have been reported. According to Hintzen *et al.*,[11] the variations in Ca-α-sialon's cell dimensions obey the following equations:

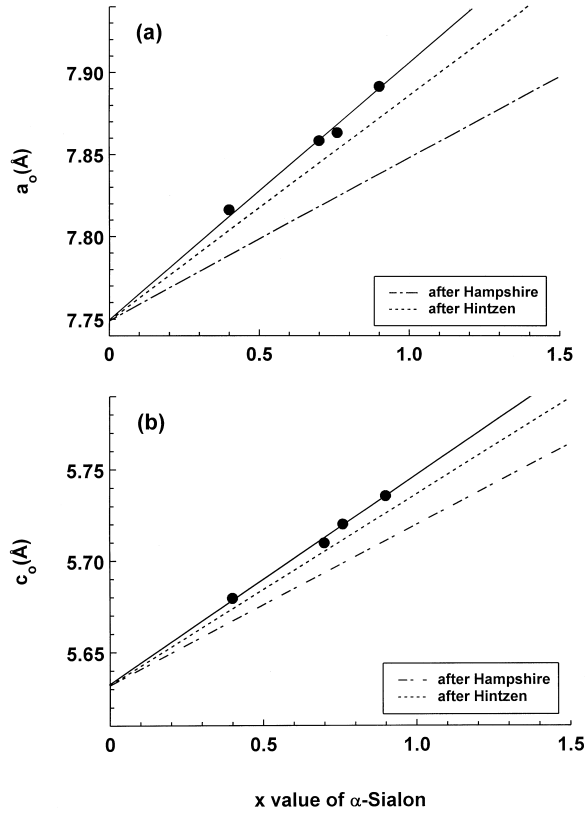

Fig. 4. Cell dimensions versus actual α-sialon compositions: (a) *a* axis; (b) *c* axis.

$$a_o(\text{Å}) = 7{\cdot}749 + 0{\cdot}0023\, n + 0{\cdot}0673\, m \qquad (3)$$

$$c_o(\text{Å}) = 5{\cdot}632 - 0{\cdot}0054\, n + 0{\cdot}0550\, m \qquad (4)$$

Obviously, for the same substitutions, eqns (3) and (4) give bigger cell dimensions than the Hampshire's equations. For comparison with the present data, the lines representing Hintzen and Hampshire's equations for the special compositions on the line of Si_3N_4-(CaO:3AlN ($Ca_xSi_{12-x}Al_{3x}O_xN_{16-x}$, $x = 1/2\,m = n$) were also put together. It is obvious that the present data are more close to the Hintzen equations, but keep slightly higher

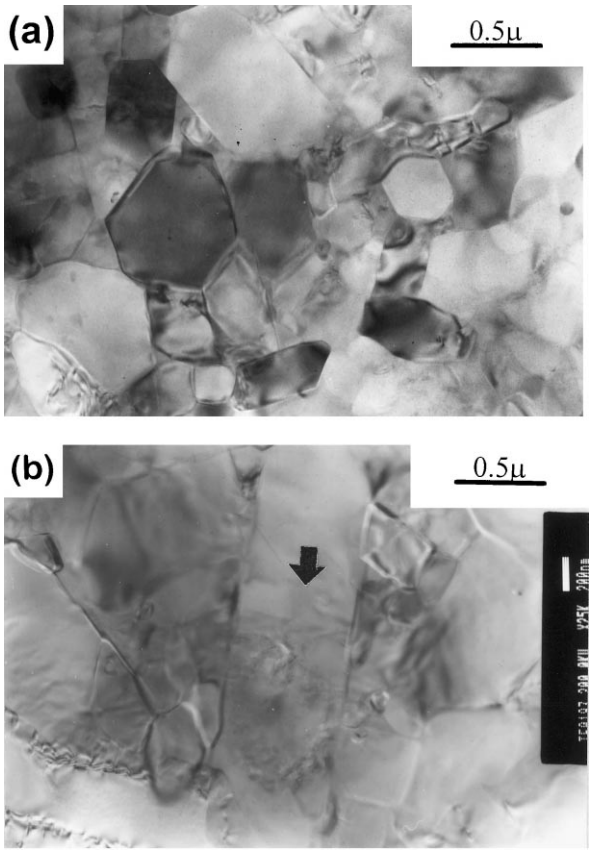

Fig. 5. TEM micrographs of the composition C60 hot-pressed at 1750°C: (a) general view of the structure; (b) showing elongated grains in some areas.

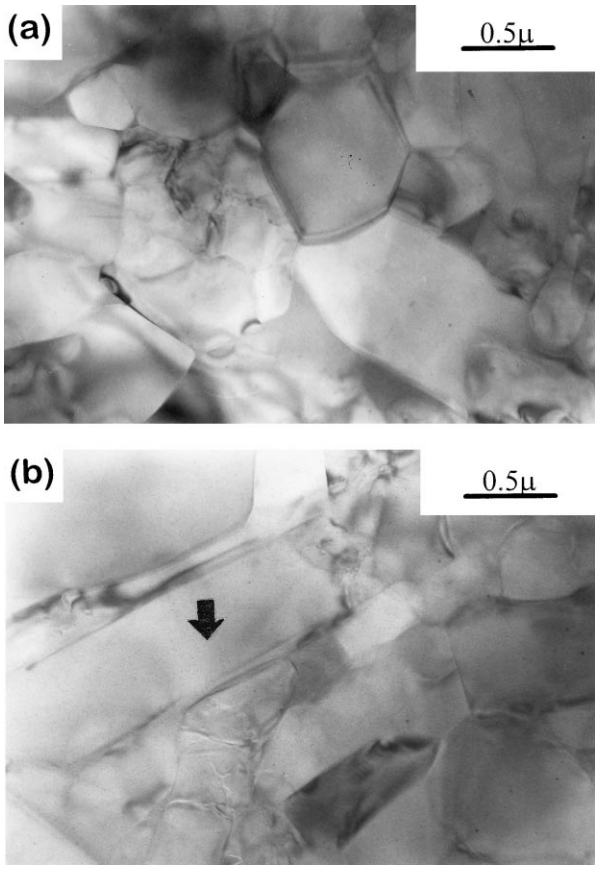

Fig. 6. TEM micrographs of the composition C140 hot-pressed at 1750°C: (a) general view of the structure; (b) showing elongated grains in some areas.

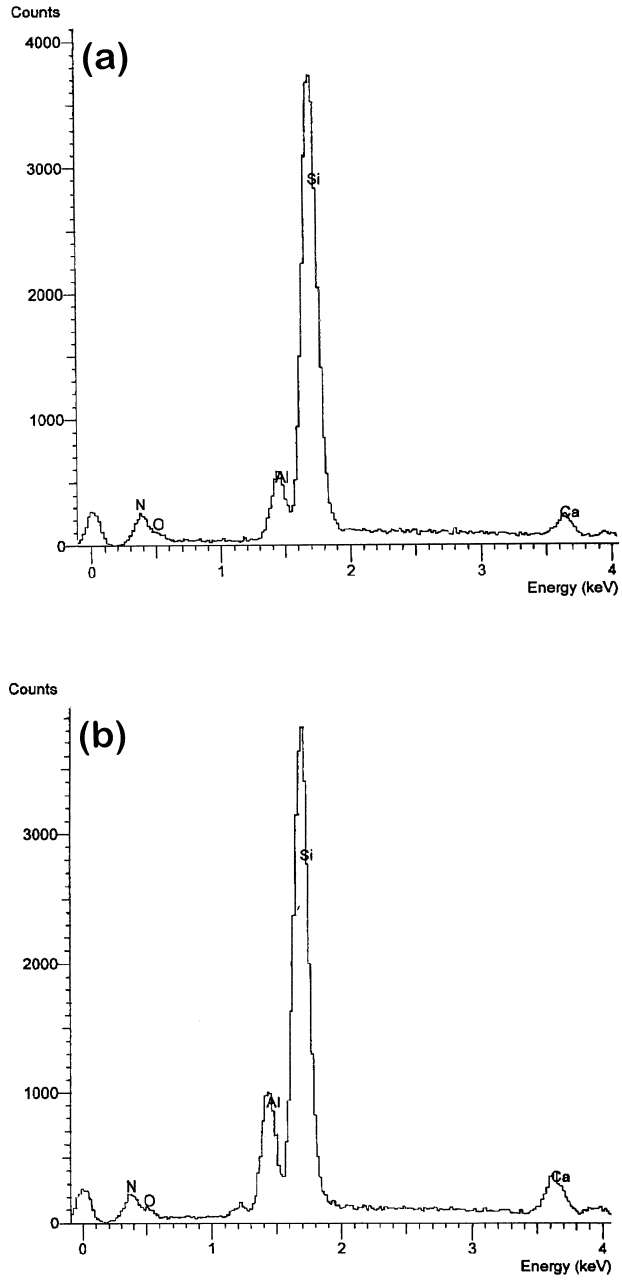

Fig. 7. EDAX spectra of the elongated grains: (a) as shown in Fig. 5(b); (b) as shown in Fig. 6(b).

slopes. The expansions of cell dimensions observed in the present work can be figured out as

$$\Delta a_o = 0{\cdot}156x \tag{5}$$

$$\Delta c_o = 0{\cdot}115x \tag{6}$$

The corresponding expansions transformed from [eqns (1–4)] are $\Delta a_o = 0{\cdot}099\ x$, $\Delta c_o = 0{\cdot}088\ x$ and $\Delta a_o = 0{\cdot}1369x$, $\Delta c_o = 0{\cdot}1046x$, respectively. Based on the present results and the Hintzen's work, Ca^{+2} entering α' structure will cause bigger expansions than the other elements and the actual $Ca^{+}2$ content in the α' is less than estimated by using Hampshire's equations. It is found by the present work that the Ca^{+2} content remaining in the glassy phase of α' material is around 30%. This

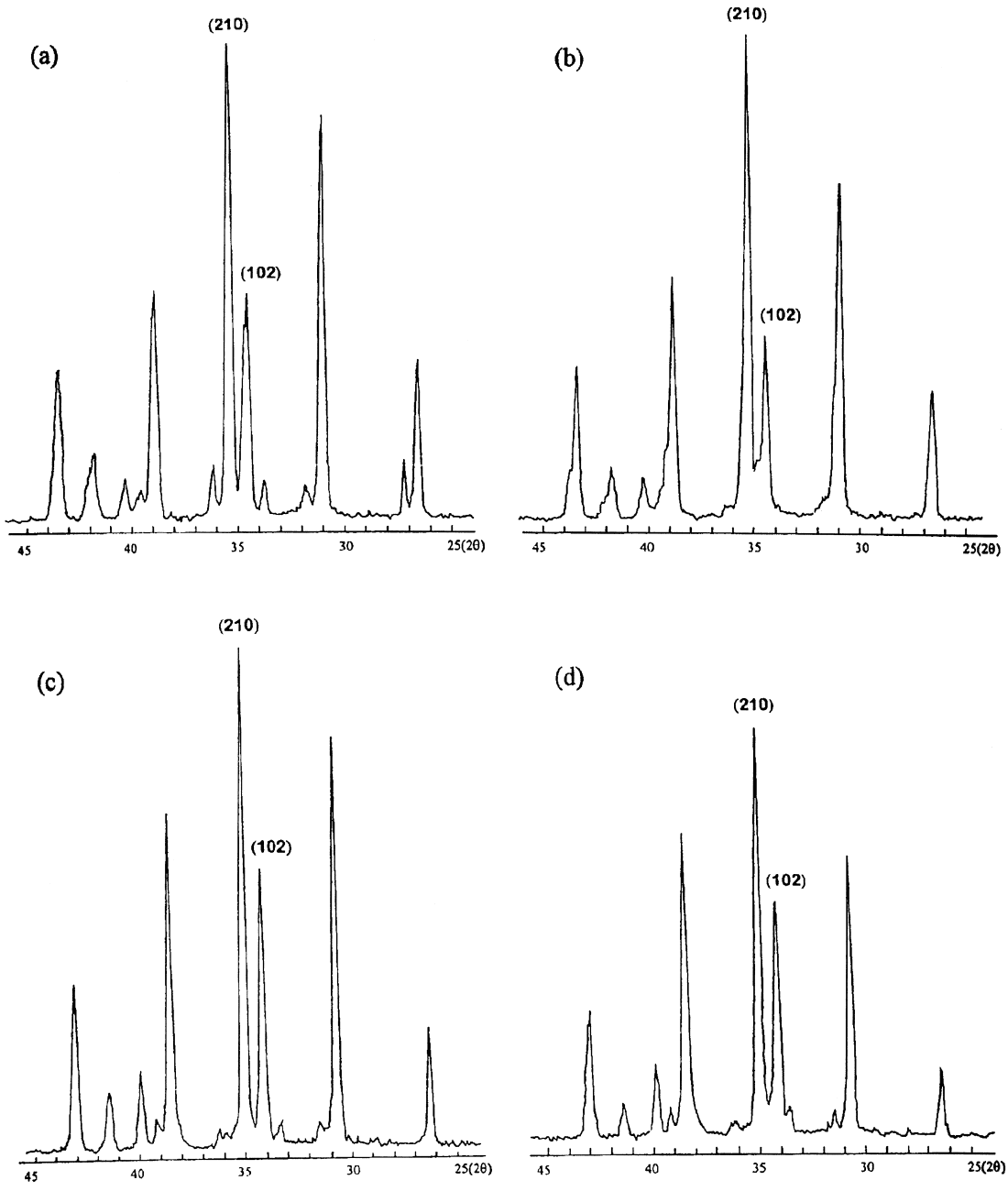

Fig. 8. Part X-ray diffraction patterns of the compositions (a) C30, (b) C60, (c) C100 and (d) C140 showing the preferred orientation of α-sialon.

might damage the high temperature performance of the material.

3.3 Microstructure and mechanical properties

It has been known that β' grains are easy to develop into aciculate and therefore, its fracture toughness is relatively high. On the other hand, α' exhibits equiaxed morphology with low fracture toughness. However, the new results[13,16–19] indicated that α' can develop into aciculate morphology under suitable conditions. The Stockholm work[16,17] indicated that in the Ln–Si–Al–O–N system, the liquid phase promotes the formation of elongated α'. Chen *et al.*[18] reported that the elongated Ln-α-sialon grains are more easy to occur by using β-Si_3N_4 as starting materials (normally α-Si_3N_4 as starting materials). In the Ca–Al–Si–O–N system, Wang *et al.*[19] first observed the preferred orientation of α' grains in hot-pressing samples and recently Hewett *et al.*[13] also reported the occurrence of elongated Ca-α-sialon grains. In the present work, the elongated α' grains were observed as well. As indicated in Figs 5(a) and (b), the microstructure of the composition C60 is composed of small equiaxed α' grains with some elongated larger α' grains. The small equiaxed grains are generally less than 1 μm and the elongated ones can develop into 2 μm in length. However, with the compositions shifting to the end member of CaO:3AlN, the α' grains becomes larger and more elongated grains occur. As indicated in Fig. 6, the α' grains in the composition C140 are larger than in the composition

C60 and the content of the elongated α' grains in C140 is also higher. In order to dispel the doubt that the elongated grains are 21 R, which normally has fiber-like morphology, the elongated grains were identified by EDAX (see Fig. 7). As shown in Fig. 7, they are all Ca-α-sialon containing increasing Ca when the compositions shifted to high x value. The elongated α' grains will give preferred orientation under hot-pressing. As expected, the preferred orientation in the present work was observed. Figure 8 shows the part X-ray diffraction patterns of the compositions C30, C60, C100, C140 taking from the specimen surface normal to the pressing direction. The normal X-ray diffraction peaks (210) and (102) of α-Si_3N_4 or α' have similar intensity.[20] However, as indicated, in all the samples the diffraction intensity of (210) peak is higher than the one of (102). These diffraction patterns show the strong evidence for the preferred orientation of the elongated α' grains. Based on the observations under TEM, it was found that the amount of elongated α' grains increases with the compositions shifting to the end member of CaO:3AlN (high x value). However, as seen in Fig. 8, the XRD intensity ratios of (210) to (102) become smaller when the compositions shift towards high x value. This is caused by the overlapped XRD peak of 21 R, which occurs in the compositions with high x value (see Table 1). The strongest X-ray diffraction peak (101) of 21 R occurs at $2\theta = 33{\cdot}99°$ and this is just overlapped with the XRD peak (102) of α' and thus makes the peak at 34° stronger. The existence of 21 R was also observed under TEM, as represented in Fig. 9. Based on our present work and the other work,[13,19] it can be drawn that in the Ca-α-sialon system the occurrence of elongated α' grains has stronger tendency than in the other systems.

The fracture toughness and hardness of the compositions hot-pressed at 1750°C are listed in Table 3. As indicated, the toughness increases with the compositions shifting towards high x value, which contain more elongated α' and 21 R. It has been known that 21 R normally exhibits fiber-like morphology. Therefore, the elongated α' grains and 21 R are of benefit to the fracture toughness enhancement. However, the hardness goes oppositely. This can be attributed to the liquid phase and 21 R. With the composition shifting to high x value, the amount of both 21 R and liquid phase increases and thus causes the hardness decrement. The relatively lower hardness of composition C30 is related with the incomplete reaction and lower density. The compositions with x value around 0·6–1 have the best combination of fracture toughness and hardness. Therefore, the best way to increase the fracture toughness is not through increasing liquid phase, which will sacrifice the other properties. It is believed that to properly optimize processing in order to make slow nucleation of α' grains would be the best way. For Ca-α-sialon, it seems to be more feasible than for Ln-α-sialon. If using β-Si_3N_4 as starting materials, the cost of both the starting powder and the processing (which needs gas pressure sintering at 1950°C) is much higher than the conventional price. Therefore, in many aspects — thermal stability, cost and microstructure control, Ca-α-sialon is a promising α' materials and more work is worthy to be carried on.

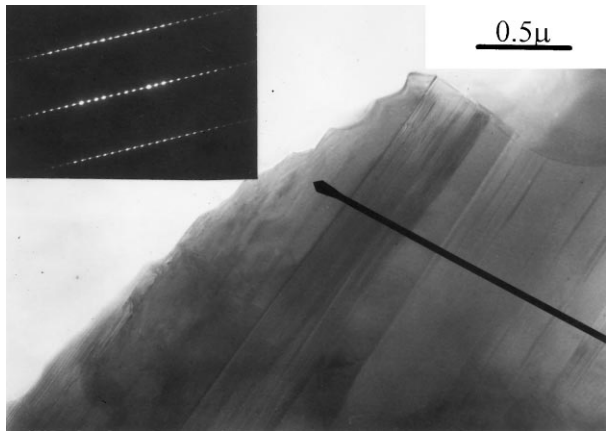

Fig. 9. TEM micrograph of 21 R in the composition C140. The corresponding electron diffraction micrograph along [100] direction of 21 R is shown on the top left corner.

Table 3. Mechanical properties of Ca-α' hot pressed at 1750 C/1 h

Sample No.	*Phases present*	Hv_{10}	K_{1c} $(MPa.m^{1/2})$
C30	α' s; β' mw; α w	1886	4·4
C60	α' s; α tr.	1975	5·1
C100	α' s; 21 R vw	1815	5·6
C140	α' s; 21 R w	1767	5·5
C160	α' s; 21 R mw	1638	5·6
C180	α' s; AlN m; 21 R w	1550	5·8

4 Conclusions

Ca-α-sialon ($Ca_xSi_{12-(m+n)}Al_{m+n}O_nN_{16-n}$, $x = m/2 = n$) with elongated α grains was fabricated by hot pressing. Although Ca-α-sialon has a rather wide solubility region, but along the $m = 2n$ line, the single phased α-sialon was observed to be restricted on x around 0·6. 21 R-polytypoid occurs in the samples when x is more than 1 and its content becomes higher when the composition shifts to higher x value. Based on the results of cell dimension and EDAX determination for Ca-α-sialon, a revised relationship between cell dimensions and

compositions was suggested, which indicates that Ca^{+2} entering α-sialon structure will cause a bigger expansion than the other elements. When x is less than 1·4, about 70% of Ca^{+2} in nominal composition enters α' structure with the remainder in grain boundary of the material. With the compositions shifting towards high x value, the elongated α-sialon grains and 21 R increase and the fracture toughness increases as well, but the hardness decreases. The best combination of the fracture toughness (5·1–5·6 MPa.($m^{1/2}$) and the hardness (1975–1815 $H_{V_{10}}$) occurs in the compositions with x value of 0·6 to 1·0.

Acknowledgements

This work has received financial support from the National Natural Science Foundation of China, Contract No.59632100 and the Bureau of Basic Science, Chinese Academy of Sciences. The authors thank Ms Y. X. Jia and Dr M. L. Ruan for their technical assistance.

References

1. Hampshire, S., Park, H. K., Thompson, D. P. and Jack, K. H., α'-Sialon ceramics. *Nature*, 1978, **274**, 880–882.
2. Lewis, M. H., Fung, R. and Taplin, D. M. R., Indentation plasticity and fracture of Si_3N_4 ceramic alloys. *Journal of Material Science*, 1981, **16**, 3437–3446.
3. Huang, Z. K., Tien, T. Y. and Yan, D. S., Subsolidus phase relationships in the Si_3N_4-AlN-rare earth oxide system. *Journal of the American Ceramic Society*, 1986, **69**, C241–242.
4. Wang, P. L., Sun, W. Y., Yen, T. S. Sintering formation behaviour of R-α'-Sialons (R = Nd, Sm, Gd, Dy, Er and Yb). *Eur. J. Solid State Inorg. Chem*, 1994, **31**, 93–104.
5. Mandal, H. and Thompson, D. P., Reversible $\alpha \Longleftrightarrow \beta$ Sialon transformation in heat-treated Sialon ceramics. *Journal of the European Ceramic Society*, 1993, **12**, 421–429.
6. Shen, Z., Ekström, T. and Nygren, M., Temperature stability of samarium-doped α'-sialon ceramics. *Journal of the European Ceramic Society*, 1996, **16**, 43–53.
7. Shen, Z., Ekström, T. and Nygren, M., Homogeneity region and thermal stability of neodymium-doped α-sialon ceramics. *Journal of the American Ceramic Society*, 1996, **79**, 721–732.
8. Huang, Z. K., Sun, W. Y. and Yan, D. S., Phase relationships of the Si_3N_4–AlN–CaO system. *J. Mater. Sci. Lett.*, 1985, **4**, 255–259.
9. Johansson, K. E., Palm, T. and Werner, P.-E., An automatic microdensitometer for X-ray powder diffraction photographs. *J. Phys. E.: Sci. Instrum.*, 1980, **13**, 1289–1291.
10. Werner, P.-E., A fortran program for least-square refinement of crystal structure cell dimension. *Arkiv fur Kemi.*, 1969, **31**, 513–516.
11. van Rutten, J. W. T., Hintzen, H. T. and Metselaar, R., Phase formation of Ca-α-sialon by reaction sintering. *Journal of the European Ceramic Society*, 1996, **16**, 995–999.
12. Sun, W. Y., Walls, P. A. and Thompson, D. P., Reaction sequences in the preparation of sialon ceramics. In *Non-oxide Technical and Engineering Ceramics*, ed. S. Hampshire. Elsevier Applied Science, London, 1986, pp. 105–117.
13. Hewett, C. L., Cheng, Y.-B., Muddle, B. C. and Trigg, M. B., Phase relationships and related microstructural observations in the Ca–Si–Al–O–N system. *J. Amer. Ceram. Soc.*, 1998, **81**, 1781–1788.
14. Sun, W. Y., Tien, T. Y. and Yen, T. S., Solubility limits of α'-sialon solid solutions in the system Si,Al,Y/N,O. *J. Amer. Ceram. Soc.*, 1991, **74**, 2547–2550.
15. Shen, Z. and Nygren, M., On the extension of the α-sialon phase area in yttrium and rare-earth doped system. *Journal of the European Ceramic Society*, 1997, **17**, 1639–1645.
16. Shen, Z., Nordberg, L.-O., Nygren, M. and Ekström, T., α-sialon grains with high aspect ratio-utopia or reality? In *Proc. Nato AST Engineering Ceramics '96—Higher Reliability through Processing*, ed. G. N., Babini. Kluwer Academic, Dordrecht, The Netherlands, 1997, pp. 169–178.
17. Nordberg, L.-O., Shen, Z., Nygren, M. and Ekström, T., On the extension of the α-sialon solid solution range and anisotropic grain growth in Sm-doped α-sialon ceramics. *Journal of the European Ceramic Society*, 1997, **17**, 575–580.
18. Chen, I-Wei and Rosenflanz, A., A tough sialon ceramic based on α-Si_3N_4 with a whisker-like microstructure. *Nature*, 1997, **389**, 701–704.
19. Wang, H., Cheng, Y.-B., Muddle, B. C., Gao, L. and Yen, T. S., Preferred orientation in hot-pressed Ca α-sialon ceramics. *J. Mater. Sci. Lett.*, 1996, **15**, 1447–1449.
20. Thompson, D. P., Powder diffraction file JCPDS-ICDD, 33–261. (Joint Committee on Powder Diffraction Standards, Swarthmore, PA, 1998).